Towards Robust Non-Fragile Control in Wind Energy Engineering

M. A. Ebrahim
Electrical Engineering Department, Faculty of Engineering, Benha University,
108 Shoubra St., P.O. Box: 11241, Cairo, Egypt.
Tel.: +20 10 04934512/2 46056399; fax: +20 2 22022310.
Corresponding author, e-mai: Mohamed.mohamed@feng.bu.edu.eg

Abstract

Blade Pitch Controller (BPC) that can cope system uncertainties is one of the most interesting topics in wind energy engineering. Therefore, this paper presents a step towards the design of robust non-fragile BPC for wind energy conversion system. The proposed approach presents all boundaries of stability region that can guarantee robust stability (RS) over a wide range of operating conditions. The proposed technique results from the complementarity of both Root-Locus and Routh-Hurwitz (RL/RH) approach. Continuous variation in the operating conditions is tackled through a new hybrid control technique based on the referential integrity of both RL/RH and Kharitonov (Kh) theorem. Simulation results confirm the effectiveness of the proposed designing approach in computing the most resilient and robust controller.

Keywords: Dynamic stability, Robustness, Resilient controllers, Kharitonov's theorem, Wind energy, Blade pitch control

1. Introduction

Wind energy, as an alternative to fossil fuels, is one of the most prominent renewable energy resources. Wind power capacity has expanded rapidly to 435 GW in February 2016 with a global growth rate of 17.2 % which was higher than in 2015 (16.4%). Wind energy production was around 5% of total worldwide electricity usage, and growing rapidly [1].

Figure 1 shows the basics of Wind Energy Conversion Systems (WECS) operation. The moving air (wind) drives Wind Turbine (WT) to convert the kinetic energy of wind into mechanical energy and then into electrical energy as illustrated in Figure 1. WECS is not just be used for generating electricity from the wind, but also about using this energy efficiently. WECS is often equipped with Blade Pitch Controller (BPC) for high-quality power generation. BPC is applied in many areas including medical, transportation, robotics, aerospace, military, and energy harvesting [2]. There are many industrial applications that the core principles of BPC are successfully applied such as control of Unmanned Aerial Vehicle (UAV), quad rotor helicopters and missile launchers which are aerodynamically unstable by their nature. The WT is often equipped with BPC for regulating turbine speed, stabilizing power extraction from wind energy and decreasing mechanical fatigue. Modeling and control of BPC system are the prerequisites of WECS for regulating maximum power and enhancing aerodynamic performance [3-4]. The complete dynamical model of WECS is very complex because it is an under-actuated, highly coupled and nonlinear system [5]. Such dynamical system is usually decomposed into generator and WT systems through controller design [6]. The complete BPC system of the real WECS is too complex. Researchers usually design BPC with simplified blade pitch model which is derived out by neglecting blade torsional dynamics [7]. In this case, the simplified blade pitch model has a relatively significant difference between the actual model. By taking the pitch servo motor, actuator, blade torsional dynamics into consideration then, the new simplified blade pitch model is more reasonable [6]. For the purpose of regulating maximum energy harvesting and minimizing mechanical stress on WECS, researchers proposed many kinds of control strategies for BPC system. Various control techniques are widely applied in BPC design, such as sliding mode control [8], robust control [9-11], fuzzy control [12], neural network control [13], PID control [14-15], and so on. Although sliding mode control achieves good performance, but it is too complex to use on a real WECS. Also, adaptive and predictive controllers need tough tuning

effort before applying in the actual system. Thanks to essential functionality and simple structure, PID is widely used in the industry up to small applications.
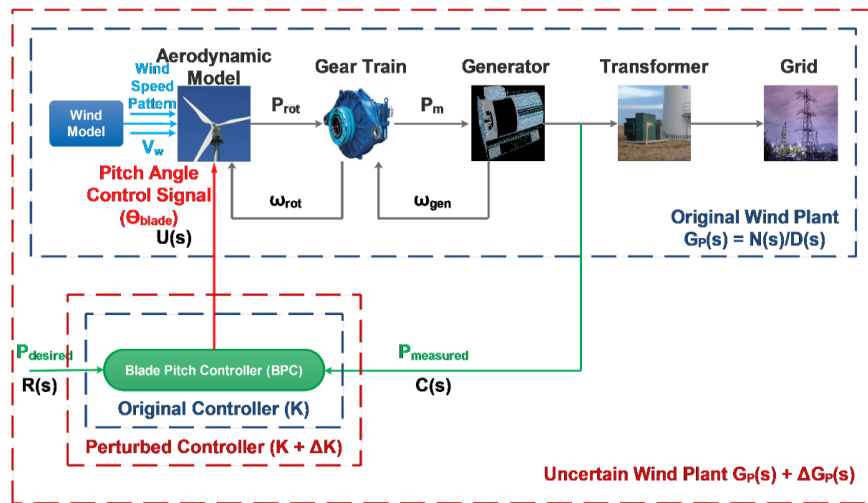

Figure 1. WECS with plant uncertainties and perturbed BPC parameters

WECS typically uses BPC to fulfill two basic functions are assigned to the BPC, which are; first, it monitors and adjusts the inclination angle of the rotor blades, thereby controlling the speed of the turbine rotor to regulate the turbine's energy production. Second, it turns the blade out of the wind in cases of high wind speeds or emergency command to avoid any damages on the WT and ensure safe operation. The standard BPC commonly used in practice is a dynamic output feedback, a lead type, with a single stage and uses the electrical power deviation ΔPe as a feedback signal [6]. Conventional fixed-parameter BPC may fail to maintain system stability over a wide range of operating conditions or at least leads to a degraded performance once the deviation from the nominal point becomes significant. Conventional fixed-parameter BPC is not enough anymore, but it has to work reliably in any environment because the ambient conditions can differ greatly in terms of temperature, humidity, and vibration. Moreover, BPC has to effectively cope with mechanical and electrical systems uncertainties imposed by continuous variation in operating points. Thus, the robustness and resiliency are crucial for the performance and operation of BPC system. Synthesis of robust BPCs has been one of the hottest topics in wind energy control system [9-11]. Over the past five decades, several methods have been developed that enable BPC to cope with parametric uncertainties in the plant dynamics [11]. Although these methods cope with uncertainty in the plant dynamics, they all assume that the derived parameters of the BPC are precise and exactly implemented. This raises an important issue that is a robust BPC can be very sensitive, or fragile, with respect to errors or perturbations in the controller coefficients and thus system instability may occur. In turn, that brings about a fundamental problem in robust control design, which has recently termed the fragility problem, and hence the design of non-fragile controller opens up as an important research topic that deserves further investigations. Up to the best of our knowledge, fragility problem of a robust BPC in wind energy systems' literature is a new topic.

The major contribution of this paper is the BPC design based on the complementarity of both Root-Locus and Routh-Hurwitz (RL/RH) approach together with Kharitonov (Kh) theorem. The proposed control technique holds the advantages of hybridized complementary approaches while overcoming their well-known practical performance limitations. The proposed controller deals with treating the misestimation problems caused by neglecting either the model/controller or the parametric uncertainties existed in WECS systems. To effectively design the resilient BPC that copes with the WECS, the modeling/parameter uncertainties are considered upon the controller design. Definitely, the proposed hybrid RL/RH - Kh technique can be ideally considered for: (i) constructing semi-graphical control approach to determine the conservative stability region that guarantee robustness, non-fragility, and resiliency of the proposed BPC;

(ii) providing better dynamic performance and stability through selecting the BPC gains inside the defined stability region; and (iii) initializing any optimization technique to overcome the undesired local optimum solutions and reduce the convergence time of simulation. Therefore, such novel technique can generally be adopted for further engineering applications.

The rest of the paper is organized as follows: Section 2 formulates the problem of the uncertainties of a simple wind energy conversion system. In Section 3, an overview of the robust and non-fragile control is presented. Necessary and sufficient constraints for characterizing all robust stabilizing BPCs are derived in Section 4. Additionally, the selection criteria of the most resilient BPC is reported. Simulation results are considered in Section 5. Finally, the conclusions and the perspectives are drawn in Section 6.

2. Wind Energy Conversion System

The WECS system considered in the paper comprises of a single WT and a grid-connected synchronous generator. The mathematical model which represents the system dynamics is given below. The system mathematical model is derived in terms of $(k_1,…,k_6)$ which are load-dependent at any operating condition in terms of active and reactive powers P and Q.

2.1. Wind Turbine Aerodynamics

The most important parts of the aerodynamic system are the WT blades, pitch servo, and the actuator. Thus, the dynamics related to these parts are considered in this paper. For the elegant form of the final state space system, the system dynamics derivation starts from the WT dynamics with notation x_7.

2.1.1. Blade Torsional Dynamics

$$\dot{x_5} = x_6 = P_{rot} \tag{1}$$

$$\dot{x_6} = -\omega_n^2 x_5 - 2\zeta\omega_n x_6 + \omega_n^2 x_7 \tag{2}$$

Where x_7 is the actuating signal for the WT blades mechanism, x_6 is the mechanical rotational power on the WT shaft, x_5 is arbitrary state determined by x_6, the aerodynamic system natural frequency, and damping coefficient are ωn and ζ respectively.

2.1.2. Pitch Servo and Actuator

$$\dot{x_7} = -\frac{1}{\tau_p} x_7 + \frac{1}{\tau_p} u \tag{3}$$

Where τ_p is the pitch servo and actuator mechanism time constant, u is the control.

2.2. Synchronous Generator

The mathematical model that describes the dynamic behavior of the synchronous generator in the rotor (dq) reference frame are given by:

$$\dot{e_q} = -\frac{k_4}{\tau_{do}'}\delta - \frac{1}{\tau_{do}'k_2}e_q + \frac{1}{\tau_{do}'}V_f \tag{4}$$

$$\dot{V_f} = -\frac{k_e k_4}{\tau_e}\delta - \frac{k_e k_6}{\tau_e}e_q - \frac{1}{\tau_e}V_f \tag{5}$$

Where e_q, V_f are the equivalent generator terminal voltage and the field voltage respectively in the dq reference frame, δ is the rotor angle of the generator, k_2, k_4, k_6 are power dependent constants, k_e, τ_e are exciter constants, τ_{do}' is the sub-transient time constant for the synchronous generator.

The mechanical dynamics are described by:

$$\dot{\omega} = \frac{\omega_o}{2h}(P_m - P_e) \tag{6}$$

$$\dot{\delta} = \omega \tag{7}$$

Where ω is the generator-angular speed, h is the WECS inertia; P_m is the mechanical power applied to the generator shaft that readily follows from (1) as:

$$P_m = K_{gt} \times P_{rot} = K_{gt} \times x_6$$

Where K_{gt} is the gear train transformation ratio, P_{rot} is the output mechanical power of the WT

The electrical power is given by:

$$P_e = k_1 \delta + k_2 e_q \tag{8}$$

Where k_1, k_2 are generator constants

2.3. Overall Dynamic Model
The overall dynamics of the system are described by (1) – (8). With the intent of writing these dynamics in a compact form, we define the state vector.

$$x = col(x_1,\ x_2,\ x_3,\ x_4,\ x_5,\ x_6,\ x_7) := col(\delta,\ \omega,\ e_q,\ V_f,\ x_5,\ x_6,\ x_7) \tag{9}$$

Define the constants:

$$J := \frac{\omega_o}{2h},\ C_1 := \frac{k_4}{\tau'_{do}},\ C_2 := \frac{1}{\tau'_{do}k_2},\ C_3 := \frac{1}{\tau'_{do}},\ C_4 := \frac{k_e k_4}{\tau_e},\ C_5 := \frac{k_e k_6}{\tau_e},\ C_6 := \frac{1}{\tau_e},\ C_7 := \omega_n^2,$$
$$C_8 := 2\zeta\omega_n,\ C_9 := \frac{1}{\tau_p}$$

Using this notation, the system state equations may be written as:

$$
\begin{aligned}
\dot{x}_1 &= x_2 \\
\dot{x}_2 &= J\big(-k_1 x_1 - k_2 x_3 + K_{gt} \times x_6\big) \\
\dot{x}_3 &= -C_1 x_1 - C_2 x_3 + C_3 x_4 \\
\dot{x}_4 &= -C_4 x_1 - C_5 x_3 + C_6 x_4 \\
\dot{x}_5 &= x_6 \\
\dot{x}_6 &= -C_7 x_5 - C_8 x_6 + C_7 x_7 \\
\dot{x}_7 &= -C_9 x_7 + C_9 u
\end{aligned}
\tag{10}
$$

Where the wind speed is seen as an external signal, and u is the control signal

3. Control Problem formulation
The main control target is to operate the WECS at its optimal power and minimizing the mechanical stresses on the aerodynamic system. To translate this objective into a standard, mathematically tractable problem, the system dynamics are represented by seven non-linear differential equations given in (10) and the system data in the Appendix A. The system model is shown in Figure 1. The system open-loop Transfer Function (TF) is determined via block diagram reduction approach for the system of equations given in (10). The model parameters $(k_1,\ldots,k_6)$ are load-dependent and have to be computed at each operating point defined by the active and reactive powers (P and Q) respectively. Therefore, the TF is load-dependent. Hence, it is more convenient to accomplish the design of BPC.

At any operating point, such TF has a general form of:

$$G_P(s) = \frac{\Delta P_e}{\Delta U} = \frac{b_2 s^2 + b_1 s + b_0}{a_7 s^7 + a_6 s^6 + a_5 s^5 + a_4 s^4 + a_3 s^3 + a_2 s^2 + a_1 s + a_0} \tag{11}$$

The coefficients a_0, a_1, a_2, a_3, a_4, a_5, b_0, b_1, and b_2 vary according to a vector ρ which consists of two independent quantities P and Q (i.e., $\rho \epsilon [P\ Q]$). The coefficients a_6 and a_7 are

always constant and independent of generator loading. Any change in P, Q leads to corresponding changes in a_0, a_1, a_2, a_3, a_4, a_5, b_0, b_1, and b_2. If P and Q vary over their prescribed intervals, i.e. $P\epsilon[P^- \ P^+]$ and $Q\epsilon[Q^- \ Q^+]$, a family of plants rather than a nominal plant are described through Equation 11. Since a_0, a_1, a_2, a_3, a_4, a_5, b_0, b_1, and b_2 depend simultaneously on ρ, the plant model can be approximated by the following interval plant:

$$a_5 = [a_5^- \ a_5^+], a_4 = [a_4^- \ a_4^+], a_3 = [a_3^- \ a_3^+], a_2 = [a_2^- \ a_2^+], a_1 = [a_1^- \ a_1^+], a_0 = [a_0^- \ a_0^+] \quad (12)$$

$$b_2 = [b_2^- \ b_2^+], b_1 = [b_1^- \ b_1^+], b_0 = [b_0^- \ b_0^+] \quad\quad\quad\quad\quad\quad (13)$$

Where:

$$[a_i^- \ a_i^+] = [\min_{\substack{P\in[P^- \ P^+], \\ Q\in[Q^- \ Q^+]a_i}} \ / \ \max_{\substack{P\in[P^- \ P^+], \\ Q\in[Q^- \ Q^+]a_i}}], i = 0,1,\ldots,5$$

$$[b_i^- \ b_i^+] = [\min_{\substack{P\in[P^- \ P^+], \\ Q\in[Q^- \ Q^+]b_i}} \ / \ \max_{\substack{P\in[P^- \ P^+], \\ Q\in[Q^- \ Q^+]b_i}}], i = 0,1,2$$

The robust stability of the interval plant is usually tackled via the celebrated Kharitonov theorem. However, some conservation is introduced because such interval plant is a hypothetical one. The power systems are time variant, and their minimums are not simultaneously guaranteed to be reached [16]. This paper aims at treating this problem through the proposed hybrid RL/RH - Kh approach.

4. Robustness versus non-fragility: an overview

Since WECS has many uncertainties as mentioned in literature, therefore the robust design is crucial for the system performance. WECS needs a controller K which internally stabilizes plant Gp with additive uncertainties ΔG_p ($G_p\pm\Delta G_p$) as indicated in Figure 1 and satisfies a given performance measure [17-19]. Various design techniques for robust control design are presented in [19-21]. Most of the research work is devoted to the structured uncertainties whose exact values are known. These algorithms do not incorporate the problems associated with the implementation of uncertain controllers.

The effect of controller uncertainties in the application of robust controllers in linear dynamical systems was addressed as fragility problem. It is, therefore, crucial for various practical purposes to restrict attention to structured uncertainties in the controller's design. Therefore, a more realistic robustness problem would be the one incorporating both plant uncertainties and BPC uncertainties as illustrated in Figure 1. Recent synthesis methods are developed to overcome the fragility problem and to guarantee good compromise between optimality and fragility [18]. The proposed hybrid RL/RH – Kh approach can be led to reach adequate parameterization of the BPC.

4.1. Robust BPC Design
4.1.1. Necessary and Sufficient Stability Constraints

Consider the feedback control system shown in Figure 1; it has a characteristic polynomial given by:

$$sD(s) + (k_d s^2 + k_p s + k_i)N(s) = 0 \quad\quad\quad (14)$$

Where:

$$D(s) = d_7 s^7 + d_6 s^6 + d_5 s^5 + d_4 s^4 + d_3 s^3 + d_2 s^2 + d_1 s + d_0$$
$$N(s) = n_2 s^2 + n_1 s + n_0$$

Supposing:

$$c_8 = d_7, \qquad c_7 = d_6, \qquad c_6 = d_5, \qquad c_5 = d_4, \qquad c_4 = d_3 + n_2 k_d,$$

$$c_3 = d_2 + n_2 k_p + n_1 k_d = c_{30} + c_{31} k_p + c_{32} k_d,$$

$$c_2 = d_1 + n_2 k_i + n_1 k_p + n_0 k_d = c_{20} + c_{21} k_i + c_{22} k_p + c_{23} k_d,$$

$$c_1 = d_0 + n_1 k_i + n_0 k_p = c_{10} + c_{11} k_i + c_{12} k_p,$$

Equation (14) can be rewritten as:

$$c_8 s^8 + c_7 s^7 + c_6 s^6 + c_5 s^5 + c_4 s^4 + c_3 s^3 + c_2 s^2 + c_1 s + c_0 = 0$$

The PID based BPC is a three-term output-feedback controller. The characterization of the robust PID controllers necessitates the determination of the values of k_p, k_i, and k_d for which Equation (14) is Hurwitz [16] . To select appropriate values for these three-term output-feedback controller gains, the stable operating region where the system is stable should be determined. The stable operating region can be determined by reaching K_p and K_i as a function of K_d. The RL technique is used for identifying the stability boundaries of K_d through only sixteen polynomials according to Kharitonov theorem. Figure 2 shows the stability limits of Kd. Here, the stability region shrinks as K_d increases. A low value of K_d is therefore desired.
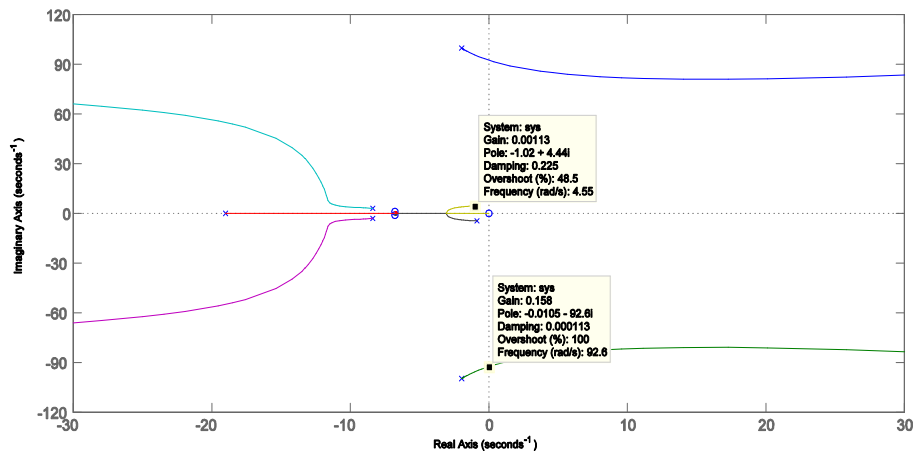

Figure 2. Stability boundaries for k_d (k_d = [0.00113 0.158])

The Routh-Hurwitz criterion is considered for deducing the necessary set of polynomial inequalities that result in sufficient stability constraints, such as:

$$
\begin{array}{c|ccccc}
s^8 & c_8 & c_6 & c_4 & c_2 & c_0 \\
s^7 & c_7 & c_5 & c_3 & c_1 & \\
s^6 & R_{61} & R_{62} & R_{63} & R_{64} & \\
s^5 & R_{51} & R_{52} & R_{53} & & \\
s^4 & R_{41} & R_{42} & R_{43} & & \\
s^3 & R_{31} & R_{32} & & & \\
s^2 & R_{21} & R_{22} & & & \\
s^1 & R_{11} & & & & \\
s^0 & R_{01} & & & &
\end{array}
$$

Where:

$$R_{61} = c_7 c_6 - c_8 c_5, \qquad R_{62} = c_7 c_4 - c_8 c_3, \qquad R_{63} = c_7 c_2 - c_8 c_1, \qquad R_{64} = c_7 c_0$$

$$R_{51} = c_5 R_{61} - c_7 R_{62}, \qquad R_{52} = c_3 R_{61} - c_7 R_{63}, \qquad R_{53} = c_1 R_{61} - c_7 R_{64}$$

$$R_{41} = R_{51} R_{62} - R_{52} R_{61}, \qquad R_{42} = R_{51} R_{63} - R_{53} R_{61}, \qquad R_{43} = R_{51} R_{64}$$

$$R_{31} = R_{41} R_{52} - R_{42} R_{51}, \qquad R_{32} = R_{41} R_{53} - R_{43} R_{51}$$

$$R_{21} = R_{31} R_{42} - R_{32} R_{41}, \qquad R_{22} = R_{31} R_{43}$$

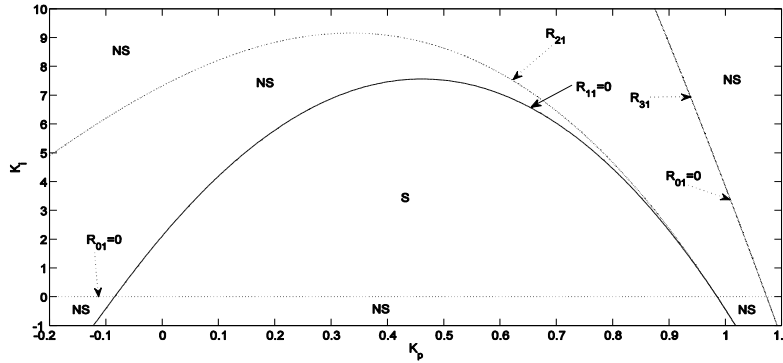$$R_{11} = R_{21} R_{32} - R_{22} R_{31}$$

$$R_{01} = R_{11} R_{22}$$

Figure 3. Routh-Hurwitz stability boundaries for P=0.8pu and Q=0.4pu

The stability boundaries are simply expressed as: $R_{i1}=0$, for i=0,1,…,6 where stability boundaries are zero-equalities. The positivity of R_{51} is ensured iff $k_d > \{c_7(c_7 c_{40} - c_3 c_{30} - c_3 c_{32} k_p) - c_5 R_{61}\}/c_7(c_3 c_{31} - c_7 c_{41})$ which in turn makes $R_{01}>0$ feasible. A test point at P=0.8pu, Q=0.4pu is considered to illustrate the stability boundaries shown in Figure 3. From Figure 3, the instability and stability regions ("Unstable" and "Stable") can be easily identified. Clearly, the stability region is completely bounded by the constraint $R_{01}=0$ (dotted- line) which is a subset of that bounded by $R_{11}=0$ (solid-line). The system within the ranges of P and Q have a steadily load flow solution (i.e., iterative load flow per condition). As a result, these ranges are mapped into controller parameters-plane of K_p - K_i. Two approaches are proposed to study the effect of variations P and Q on the reached stability region: The image-set polynomials and Kharitonov polynomials approaches. The number of polynomials in the former approach mainly depends on the step size selected to scan the intervals of P and Q. The latter approach utilizes only sixteen polynomials according to Kharitonov theorem.

4.1.2. Image-set polynomials

Appropriate step size should be considered for plotting the stability regions of different plants in the operating range of P and Q. The choice of the step is arbitrary chosen to produce clear defined stability boundaries. For the ranges P= [0.4 1.0] and Q= [0.0 0.5], a step size of 0.05 is considered for P and Q. The step size is chosen to ensure the highest accuracy in this case study which would be proven through simulation results. The stability regions of these ranges are illustrated in Figure 4. All stabilizing controllers that guarantee robust stability over these ranges result from the intersection of these regions.

Remark: a certain stability region in the controller parameter plane can be attained using image-set polynomials. However, it requires plotting the stability boundaries of 143 plants that cover the full ranges of P and Q with the specified step size. Therefore, the relatively high and time consumption are the main drawbacks of this approach.
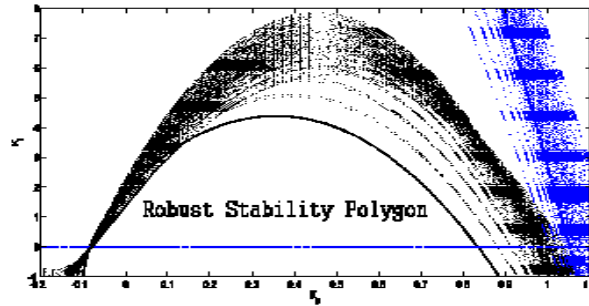
Figure 4. Stability regions for P=[0.4 1.0] and Q=[0.0 0.5]

3.1.3. Kharitonov polynomials

Only sixteen vertex plants have to be considered to guarantee the controller robustness under load uncertainties. Necessary and sufficient conditions for robust stability of according to Kharitonov theorem are discussed in [22 - 24].

Definition 1. The interval polynomial is a set of real polynomial f nth degree of the form of $P(s) = a_0 + a_1 s + a_2 s^2 + \ldots + a_n s^n$, where the coefficients vary over independent intervals i.e. $a_0 = \left[\underline{a_0}\ \overline{a_0}\right]$, $a_1 = \left[\underline{a_1}\ \overline{a_1}\right]$, $a_2 = \left[\underline{a_2}\ \overline{a_2}\right]$,..., $a_n = \left[\underline{a_n}\ \overline{a_n}\right]$.

Theorem 1. Each polynomial in the interval family f is Hurwitz-stable iff the following Kharitonov polynomials are Hurwitz-stable (proof in [22 - 24]):

$$K^1(s) = \underline{a_0} + \underline{a_1}s + \overline{a_2}s^2 + \overline{a_3}s^3 + \underline{a_4}s^4 + \underline{a_5}s^5 + \overline{a_6}s^6 + \ldots$$

$$K^2(s) = \overline{a_0} + \overline{a_1}s + \underline{a_2}s^2 + \underline{a_3}s^3 + \overline{a_4}s^4 + \overline{a_5}s^5 + \underline{a_6}s^6 + \ldots$$

$$K^2(s) = \overline{a_0} + \underline{a_1}s + \underline{a_2}s^2 + \overline{a_3}s^3 + \overline{a_4}s^4 + \underline{a_5}s^5 + \underline{a_6}s^6 + \ldots$$

$$K^2(s) = \underline{a_0} + \overline{a_1}s + \overline{a_2}s^2 + \underline{a_3}s^3 + \underline{a_4}s^4 + \overline{a_5}s^5 + \overline{a_6}s^6 + \ldots$$

Applying this theorem to the WECS, whose parameters defined by 12 and 13, the controller has to stabilize the following vertex plants simultaneously:

$$sD(s) + \left(k_d s^2 + k_p s + k_i\right)N(s) = 0, \quad i = 1,2,3,4, \quad j = 1,2,3,4$$

Sixteen vertex polynomials are termed as $\Delta_i = 1,2,3,\ldots,16$ and given in the appendix.
The boundaries of each coefficient are computed for the predefined ranges of P and Q as:

$d_7 = [1\ 1]$, $d_6 = [47.171\ 47.171]$, $d_5 = [10791\ 10818]$, $d_4 = [437755\ 438790]$, $d_3 = [6.205e+6\ 6.4902e+6]$,

$d_2 = [3.3709e+7\ 4.5144e+7]$, $d_1 = [8.9366e+7\ 2.2286e+8]$, $d_0 = [3.1132e+8\ 6.1206e+8]$,

$n_2 = [3.4897e+7\ 9.7385e+7]$, $n_1 = [8.4076e+8\ 2.2124e+9]$, $n_0 = [3.6923e+9\ 7.2591e+9]$.
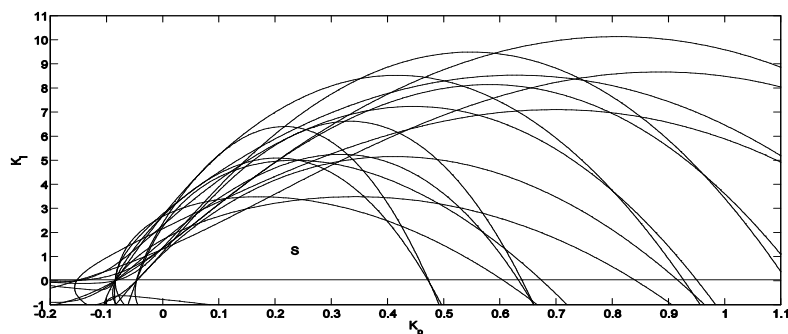

Figure 5. Stability region for Kharitonov plants

Accordingly, the stability regions of the sixteen polynomials are shown in Figure 5.

4.2. Non-fragility analysis

To enhance non-fragility of a robust blade pitch controller shown in Figure 1, robust stability basin is searched for the point $(k_p(0), k_i(0), k_d(0))$ that allows for maximum perturbations in the controller parameters $(\Delta k_p, \Delta k_i, \Delta k_d)$. Characterization of all robust controllers is firstly developed where the convex polygon is shown in figure. 6 characterizes all robust stabilizing BPCs.

In this paper, the most non-fragile BPC has selected at the center of the maximum area inscribed rectangle that permits for maximum dependent variations in the parameters of the controller. It is evident from figure. 6 that the stability region by Kharitonov polynomials is a subset of that obtained by image-set polynomials, and therefore the maximum area inscribed rectangle of the latter is larger than that of the first. Hereafter, the maximum allowable ranges for K_p and K_i while $K_d \approx [0.00113 \ 0.158]$ are given by $K_p \approx [0.1 \ 0.625]$, $K_i \approx [0.0 \ 3.0]$ for image-set polynomials and given by $K_p \approx [0.1 \ 0.4]$, $K_i \approx [0.0 \ 2.45]$ for Kharitonov polynomials. The most resilient controller is considered at the center of the box of controller parameters as follows:

Image-set polynomials: $K_p(0) = 0.3625$, $K_i(0) = 1.500$, $K_d(0) = 0.079565$
Kharitonov polynomials: $K_p(0) = 0.2500$, $K_i(0) = 1.125$, $K_d(0) = 0.079565$
These values can permit for maximum allowable controller perturbations.

5. Stability Regions Classification and Verification

To properly verify the theoretical findings of the proposed hybrid RL/RH - Kh approach, different local (typically gradient-based) or global (typically non-gradient based or evolutionary) optimization techniques are considered to check the stability region. For this purpose, four various performance indices are used such as Integral Absolute Error (IAE), Integral Square Error (ISE), Integral Time Absolute Error (ITAE) and Integral Time Square Error (ITSE) [25 – 35]. In this study, the commonly used optimization techniques in engineering optimization applications are considered such as Zeigler Nicolas (ZN), Simplex Algorithm (SA) and Genetic Algorithm (GA) [25 – 29].

These different most-used metaheuristic optimization techniques are considered for reaching the optimal PID-BPC gains. Reaching optimal gain values inside the pre-specified stability zone defined by the hybrid RL/RH - Kh approach explains the technique's capability towards providing an optimal stability area. In such area, the BPC will be robust, non-fragile and resilient. As depicted in Figure 6, there is a slight difference among robustness, non-fragility, and resiliency. From Figure 6, it is clear that the resiliency region is a subset of the non-fragility region. Both latter located inside the robust stability region. Therefore, the robustness stability property of the resilient one is better than that of the non-fragile one. Hereafter, the most resilient BPC parameters are the most robust non-fragile ones.

For validating the effectiveness of the proposed hybrid RL/RH - Kh approach as a control design tool, the different metaheuristic optimization techniques are suggested for the optimal BPC gains determination.

The efficiency of the hybrid RL/RH - Kh approach is confirmed through the comprehensive comparative study using both conventional and metaheuristic based control design techniques considering the commonly used performance indices. From Figure 6, it is clear that all optimal BPC gains are located inside the predefined stability region. Both SA and ZN provide robust BPC gains inside the conservative stability region (B).

From Figure 6, the use of GA technique allows reaching robust and non-fragile BPC gains inside the maximum area inscribed within the stability region (B). However, the GA fails to provide the best resilient BPC. The GA technique is better than other proposed techniques in attaining the most robust, non-fragile BPC. Therefore, the GA is the nearest AI based metaheuristic optimization techniques capable of reaching the resiliency zone.

From Figure 6, all BPC parameters obtained by both classical and AI based metaheuristic optimization techniques always located within the pre-specified stability region presented by RL/RH - Kh.

Table 1, presents a comparative assessment and analysis of two representative optimization methods for BPC-PID determination. The optimal gains for BPC system using standard ZN are $K_p = 0.083$, $K_i = 0.341$, $K_d = 0.08$. From Table 1, the ITSE index has better tuning

performance due to its minimum objective function and less computation time. The SA and ZN techniques failed in finding either resilient or non-fragile BPC. Clearly, the robust and/or non-fragile BPC is not necessarily considered as a resilient one as illustrated in Table 2.
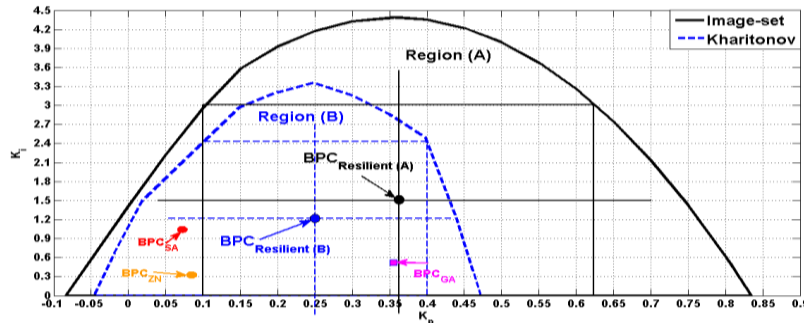

Figure 6. Maximum-area inscribed rectangular with K_d = [0.00113   0.158]

Table 1. A comparative assessment and analysis of different optimization methods for BPC-PID

	SA				GA			
	IAE	ISE	ITAE	ITSE	IAE	ISE	ITAE	ITSE
K_p	0.109	0.087	0.074	0.108	0.320	0.388	0.361	0.361
K_i	1.612	2.755	1.005	1.802	0.718	0.541	0.528	0.528
K_d	0.054	0.096	0.034	0.060	0.078	0.091	0.039	0.039
Obj. fun.	0.094	0.043	0.014	0.002	0.067	0.067	0.067	0.067
Time	0.457	0.456	0.455	0.450	0.866	0.738	0.773	0.703

Table 2. A comparative assessment and analysis for all proposed BPC-PID controllers

	Robust	Non-fragile	Resilient
BPCResilient(A)	√	√	√√√
BPCResilient(B)	√	√	√√√√
BPCSA	√	✕	✕
BPCZN	√	✕	✕
BPCGA	√	√	√
BPCABC	√	√	√√

6. Simulation Results
6.1. Robust Stability of Exact Controller {Kp(0) , Ki(0), Kd(0)}.
The most resilient controller is selected as $K_p(0)$ =0.3625, $K_i(0)$ =1.5, $K_d(0)$ =0.079565. The effectiveness of such controller, to guarantee robust stability over the entire range of P and Q is depicted in Figure. 7.

6.2. Robust Stability of ±30% Perturbed Controller
The gains of the exact controller are reduced by 30%, i.e. K_p =0.7Kp(0), K_i =0.7$K_i(0)$, K_d =0.7$K_d(0)$. The effectiveness of the perturbed controller, to guarantee robust stability over the entire range of P and Q is depicted in Figure 7.
For the modeling and control of the system's stability, the resilient BPC is simulated at an operating point given by P=0.9pu and Q=0.4pu. In this paper, mechanical power disturbance and wind speed variation are considered.

5.3. Small-Signal Disturbance and Resiliency Assessment
The system response for 0.1pu step increment in the reference mechanical power at t=0.5s with full recovery after 100 ms is depicted in Figure. 7. Remarkably, the proposed BPC can enhance the system damping. In Figure. 7, explicitly, the resiliency of the proposed BPC is examined by considering the rotor angle response for the same disturbance with exact and perturbed controllers.
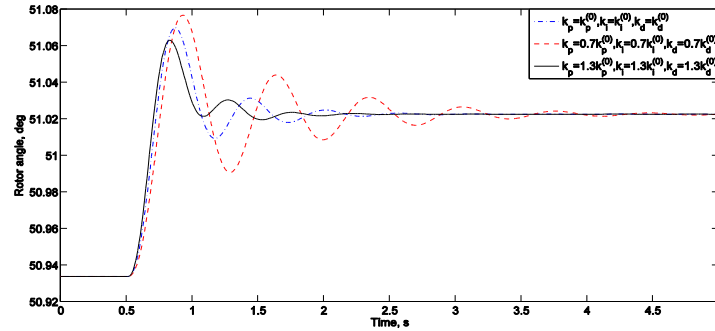
Figure 7. Rotor angle response for 0.1pu increment in torque with exact and perturbed BPCs

5.4. Large Signal Disturbance Performance Assessment
5.4.1. Robustness Assessment

To assess the effectiveness of the proposed BPC and to verify its robustness, the system dynamic behavior in the presence of significant disturbances should be verified. This consideration is as equally important as studying the system performance under small disturbance. Therefore, two wind profiles are tested; a step change and stochastic wind patterns. The wind profiles are chosen to represent large, as well as small wind guests. In Figure 8, the system is subjected to a step change wind profile. Noticeably, the proposed BPC is robust under step wind disturbance.
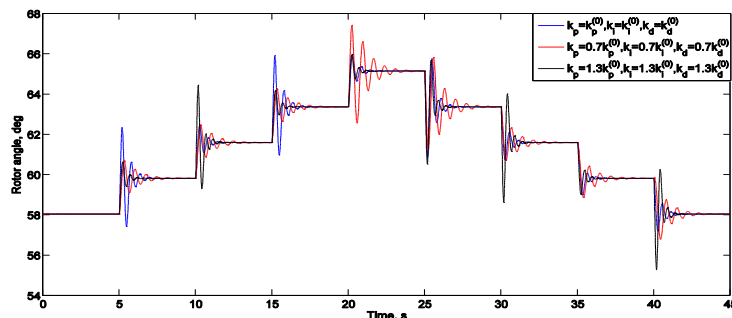
Figure 8. Rotor angle response for step change wind speed profile with exact and perturbed BPCs

5.4.2. Non-Fragility Assessment

To investigate the non-fragility property of the proposed design, the system is subjected to a stochastic wind profile. In Figure 9, it is evident that the design is non-fragile under this realistic wind profile.
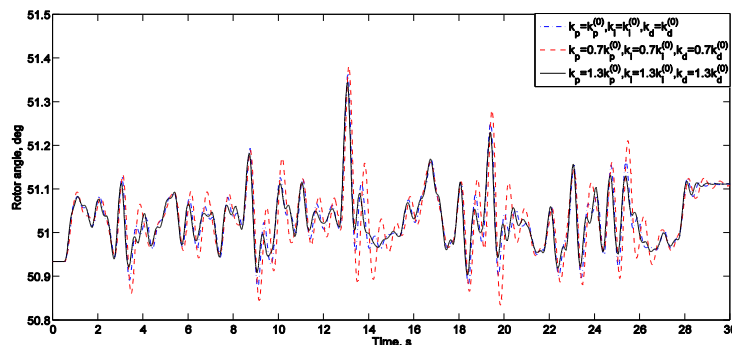

Figure 9. Rotor angle response for realistic wind speed profile with exact and perturbed BPCs

6. Conclusion

In this paper, a real wind energy conversion system had been modeled in MATLAB/SIMULINK environment. Although the network model used was simplified to some extent, the effects of the main elements of the network were considered. These elements included the wind turbine, gearbox, bus bars, transformers, and cables. The transient stability during the wind variation has been analyzed. An elegant control design approach has been presented in this paper for optimal design of the PID-BPC.

According to this research work, the single analysis using either Routh-Hurwitz criterion or Root-Locus approach was insufficient to identify the most robust and resilient controller. Referential Integrity for the results of the two analyses RH and RL (as proposed by the new approach RI-RH/RL) showed accuracy in defining the stability polygon. Based on the precious analysis attained by RI-RH/RL approach, a new hybrid Kharitonov based RI-RH/RL approach was proposed for the optimal selection of the controller parameters. Simulations results based on WECS model are carried out to reveal the effectiveness of the proposed approach. Thus, the approach used succeeded in proving its capability to select the most resilient controller.

In the forthcoming work, the author will focus on building a MATLAB toolbox for the hybrid Kharitonov based RI-RH/RL approach from which the most robust resilient region can be identified. Such region can be conveniently considered as bounded constraints area rather than a stability condition for any proposed optimization techniques used for optimal gain scheduling.

References

[1]   The World Wind Energy Association (2016). 2016 Statistics Report. WWEA.
[2]   TK Barlas, GAM van Kuik. Review of state of the art in smart rotor control research for wind turbines. *Progress in Aerospace Sciences.* 201; 46(1): 1-27.
[3]   Adomavičius V, Ramonas Č, Kepalas V. Control of Wind Turbine's Load in order to maximize the Energy Output. *Elektronika ir Elektrotechnika*. 2015; 88(8): 71-76.
[4]   Eltigani D, Masri S. Challenges of integrating renewable energy sources to smart grids: A review. *Renewable and Sustainable Energy Reviews.* 2015; 52: 770-780.
[5]   H Geng, G Yang. Linear and nonlinear schemes applied to pitch control of wind turbines. *The Scientific World Journal.* 2014; 14(1): 1-9.
[6]   MA Ebrahim, KA El-Metwally, FM Bendary, WM Mansour. Optimization of the proportional-integral-differential controller for wind power plant using particle swarm optimization technique. *International Journal Electronic Power Engineering*. 2012; 6(1): 32-37.
[7]   A Stosky, B Egart. *Robust, proactive control of wind turbines with reduced blade pitch actuation.* Proc. 5th Symposium on System Structure and Control Part of 2013 IFAC Joint Conference SSSC. Grenoble, France.
[8]   B Beltran, T Ahmed, M El Hachemi. Sliding mode power control of variable-speed wind energy conversion systems. *IEEE Trans. Energy Conversion.* 2008; 23(2): 551-558.
[9]   ASC Nandar, T Hashiguchi, T Goda, T Tsuji. Design of a coordinated robust controller of SMES and blade pitch for smart-grid power systems. *IEEJ Trans. Elect Electron Eng.* 2012; 7(1): 355-362.
[10]   Sungsu Park. A novel individual pitch control algorithm based on μ-synthesis for wind turbines. *Journal of Mechanical Science and Technology.* 2013; 28(4): 1509-1517.
[11]   C Sloth, T Esbensen, MOK Niss, J Stoustrup, PF Odgaard. *Robust LMI-based control of wind turbines with parametric uncertainties.* Proc. 18th IEEE International Conference on Control Applications Part of 2009 IEEE Multi-conference on Systems and Control. Saint Petersburg, Russia, 2009.
[12]   MA Ebrahim, KA El-Metwally, FM Bendary, WM Mansour. Transient Stability Enhancement of a Wind Energy Distributed Generation System by Using Fuzzy Logic Stabilizers. *Int. J. Wind Engineering*. 2012; 36(6): 687-700.
[13]   Yilmaz, Ahmet Serdar, Zafer Özer. Pitch angle control in wind turbines above the rated wind speed by multi-layer perceptron and radial basis function neural networks. *Expert Systems with Applications.* 2009; 36(6): 9767-9775.
[14]   Lu Q, Bowyer R, Jones BL. Analysis and design of Coleman transform-based individual pitch controllers for wind-turbine load reduction. *Wind Energy*. 2015; 18(8): 1451-1468.
[15]   H Namik, K Stol. Individual blade pitch control of a spar-buoy floating wind turbine. *IEEE Trans. Control Systems Technology.* 2014; 22(1): 214-223.
[16]   Soliman M. Parameterization of robust three-term power system stabilizers. *Electrical power systems research.* 2014; 117(1): 172-184.
[17]   P Apkarian, RJ Adams. Advanced gain-scheduling techniques for uncertain systems. *IEEE Trans. Control Systems Technology.* 1998; 6(1): 213-232.

[18] Keel LH, Bhattacharyya SP. Robust, fragile or optimal. *IEEE Trans. Automatic Control.* 1997; 42(8): 1098-1105.

[19] M Magdi. Resilient control of uncertain dynamical systems. Berlin, Heidelberg: Springer-Verlag. 2004.

[20] Soliman HM, Mahmoud MS. Resilient static output feedback power system stabilizer using PSO-LMI optimization. *Int J Syst. Contr. Comm.* 2013; 5(1): 74-91.

[21] Bhattacharyya SP, H Chapellat, Keel LH. Robust control: the parametric approach. Prentice-Hall. 1995.

[22] Soliman M. Robust non-fragile power system stabilizer. Electrical power and energy systems. 2015; 64(1): 626-634.

[23] VL Kharitonov. Asymptotic stability of an equilibrium position of a family of systems of linear differential equations. *Differential'nye Uravnenya*. 1978. 14(11): 2086-2088.

[24] Gryazina, Elena N, Boris T Polyak. Stability regions in the parameter space: D-decomposition revisited. *Automatica.* 2006; 42(1): 13-26.

[25] Ahmed M, MA Ebrahim, Ramadan HS, Becherif *M. Optimal Genetic-sliding Mode Control of VSC-HVDC Transmission Systems*. The International Conference on Technologies and Materials for Renewable Energy, Environment and Sustainability- TMREES15. 2015: 1048-1060.

[26] MA Ebrahim, Mostafa HE, Gawish SA, Bendary FM. *Design of decentralized load frequency based-PID controller using stochastic particle swarm optimization technique*. In Electric Power and Energy Conversion Systems. 2009: 1-6.

[27] Jagatheesan K, Anand B, Dey N, MA Ebrahim. *Design of Proportional-Integral-Derivative Controller Using Stochastic Particle Swarm Optimization Technique for Single-Area AGC Including SMES and RFB Units*. In Proceedings of the Second International Conference on Computer and Communication Technologies. 2016: 299-309.

[28] Jagatheesan K, Anand B, MA Ebrahim. Stochastic particle swarm optimization for tuning of PID controller in load frequency control of single area reheat thermal power system. *International Journal Electronics Power Engineering*. 2014: 33-40.

[29] MA Ebrahim, El-Metwally KA, Bendary FM, Mansour WM, Ramadan HS, Ortega R, Romero J. Optimization of Proportional-Integral-Differential Controller for Wind Power Plant Using Particle Swarm Optimization Technique. *International Journal of Emerging Technologies in Science and Engineering.* 2011.

[30] Mousa ME, Ebrahim MA, Hassan MM. Stabilizing and swinging-up the inverted pendulum using PI and PID controllers based on reduced linear quadratic regulator tuned by PSO. *International Journal of System Dynamics Applications (IJSDA).* 2015; 4(4): 52-69.

[31] Ali AM, Ebrahim MA, Hassan MM. Automatic Voltage Generation Control for Two Area Power System Based on Particle Swarm Optimization. *Indonesian Journal of Electrical Engineering and Computer Science.* 2016; 2(1): 132-144.

[32] Ebrahim MA, Elyan T, Wadie F, Abd-Allah MA. Optimal design of RC snubber circuit for mitigating transient overvoltage on VCB via hybrid FFT/Wavelet Genetic approach. *Electric Power Systems Research.* 2017; 143: 451-461.

[33] Mousa ME, Ebrahim MA, Hassan MM. *Optimal Fractional Order Proportional—Integral—Differential Controller for Inverted Pendulum with Reduced Order Linear Quadratic Regulator*. In Fractional Order Control and Synchronization of Chaotic Systems, Springer International Publishing. 2017: 225-252.

[34] Ebrahim MA, Ramadan HS. Interarea Power System Oscillations Damping via AI-based Referential Integrity Variable-Structure Control. *International Journal of Emerging Electric Power Systems.* 2016; 17(5): 497-509.

[35] Soued S, Ebrahim MA, Ramadan HSM, Becherif M. Optimal Blade Pitch Control for Enhancing the Dynamic Performance of Wind Power Plants via Metaheuristic Optimizers. *IET Electric Power Applications.* 2017.

Appendix

Table 1. Operating conditions

Infinite bus voltage	$V\infty=1$	Gear ratio	$N=37.5$
Active power	$P=0.8$	Reactive power	$Q=0.4$
Torque factor	$K_{th}=11.86$		

Table 2. System data

Transmission line resistance	R_{tl}=0	Transient d-axis reactance	X_d'=0.165
Transmission line reactance	X_{tl} =0.4	Sub-transient d-axis reactance	$X_{d''}$=0.128
Turbine speed r.p.m	N_r=40	Sub-transient q-axis reactance	$X_{q''}$=0.193
Blade radius	r_b=62.5	D-axis transient field time constant	$\tau_{do'}$=1.94212
Wind speed m/sec	V_W =10	Q-axis sub-transient field time constant	$\tau_{do''}$=0.01096
No. of poles	PP=4	Q-axis sub-transient field time constant	$\tau_{qo''}$=0.0623
Inertia constant	h=10	Angular speed of the generator (base value) [rad/sec]	ω_o=100π
Zeta	ζ=0.02	ω_n	ω_n=100
Generator armature resistance	R_a=0.0	Wind turbine filter time constant	τ_p=1/(2*2.7*π)
D-axis reactance	X_d=1.6	Exciter time constant	τ_e=0.05
Q-axis reactance	X_q=1.55	Exciter gain	K_e=50

Kharitonov polynomials for the proposed system:

$$\Delta_1 = \left(\underline{d}_7 s^8 + \underline{d}_6 s^7 + \overline{d}_5 s^6 + \overline{d}_4 s^5 + \underline{d}_3 s^4 + \underline{d}_2 s^3 + \overline{d}_1 s^2 + \overline{d}_0 s \right) + \left(k_d s^2 + k_p s + k_i \right)\left(\underline{n}_2 s^2 + \underline{n}_1 s + \overline{n}_0 \right)$$

$$\Delta_2 = \left(\overline{d}_7 s^8 + \overline{d}_6 s^7 + \underline{d}_5 s^6 + \underline{d}_4 s^5 + \overline{d}_3 s^4 + \overline{d}_2 s^3 + \underline{d}_1 s^2 + \underline{d}_0 s \right) + \left(k_d s^2 + k_p s + k_i \right)\left(\underline{n}_2 s^2 + \underline{n}_1 s + \overline{n}_0 \right)$$

$$\Delta_3 = \left(\overline{d}_7 s^8 + \underline{d}_6 s^7 + \underline{d}_5 s^6 + \overline{d}_4 s^5 + \overline{d}_3 s^4 + \underline{d}_2 s^3 + \underline{d}_1 s^2 + \overline{d}_0 s \right) + \left(k_d s^2 + k_p s + k_i \right)\left(\underline{n}_2 s^2 + \underline{n}_1 s + \overline{n}_0 \right)$$

$$\Delta_4 = \left(\underline{d}_7 s^8 + \overline{d}_6 s^7 + \overline{d}_5 s^6 + \underline{d}_4 s^5 + \underline{d}_3 s^4 + \overline{d}_2 s^3 + \overline{d}_1 s^2 + \underline{d}_0 s \right) + \left(k_d s^2 + k_p s + k_i \right)\left(\underline{n}_2 s^2 + \underline{n}_1 s + \overline{n}_0 \right)$$

$$\Delta_5 = \left(\underline{d}_7 s^8 + \underline{d}_6 s^7 + \overline{d}_5 s^6 + \overline{d}_4 s^5 + \underline{d}_3 s^4 + \underline{d}_2 s^3 + \overline{d}_1 s^2 + \overline{d}_0 s \right) + \left(k_d s^2 + k_p s + k_i \right)\left(\overline{n}_2 s^2 + \overline{n}_1 s + \underline{n}_0 \right)$$

$$\Delta_6 = \left(\overline{d}_7 s^8 + \overline{d}_6 s^7 + \underline{d}_5 s^6 + \underline{d}_4 s^5 + \overline{d}_3 s^4 + \overline{d}_2 s^3 + \underline{d}_1 s^2 + \underline{d}_0 s \right) + \left(k_d s^2 + k_p s + k_i \right)\left(\overline{n}_2 s^2 + \overline{n}_1 s + \underline{n}_0 \right)$$

$$\Delta_7 = \left(\overline{d}_7 s^8 + \underline{d}_6 s^7 + \underline{d}_5 s^6 + \overline{d}_4 s^5 + \overline{d}_3 s^4 + \underline{d}_2 s^3 + \underline{d}_1 s^2 + \overline{d}_0 s \right) + \left(k_d s^2 + k_p s + k_i \right)\left(\overline{n}_2 s^2 + \overline{n}_1 s + \underline{n}_0 \right)$$

$$\Delta_8 = \left(\underline{d}_7 s^8 + \overline{d}_6 s^7 + \overline{d}_5 s^6 + \underline{d}_4 s^5 + \underline{d}_3 s^4 + \overline{d}_2 s^3 + \overline{d}_1 s^2 + \underline{d}_0 s \right) + \left(k_d s^2 + k_p s + k_i \right)\left(\overline{n}_2 s^2 + \overline{n}_1 s + \underline{n}_0 \right)$$

$$\Delta_9 = \left(\underline{d}_7 s^8 + \underline{d}_6 s^7 + \overline{d}_5 s^6 + \overline{d}_4 s^5 + \underline{d}_3 s^4 + \underline{d}_2 s^3 + \overline{d}_1 s^2 + \overline{d}_0 s \right) + \left(k_d s^2 + k_p s + k_i \right)\left(\overline{n}_2 s^2 + \underline{n}_1 s + \underline{n}_0 \right)$$

$$\Delta_{10} = \left(\overline{d}_7 s^8 + \overline{d}_6 s^7 + \underline{d}_5 s^6 + \underline{d}_4 s^5 + \overline{d}_3 s^4 + \overline{d}_2 s^3 + \underline{d}_1 s^2 + \underline{d}_0 s \right) + \left(k_d s^2 + k_p s + k_i \right)\left(\overline{n}_2 s^2 + \underline{n}_1 s + \underline{n}_0 \right)$$

$$\Delta_{11} = \left(\overline{d}_7 s^8 + \underline{d}_6 s^7 + \underline{d}_5 s^6 + \overline{d}_4 s^5 + \overline{d}_3 s^4 + \underline{d}_2 s^3 + \underline{d}_1 s^2 + \overline{d}_0 s \right) + \left(k_d s^2 + k_p s + k_i \right)\left(\overline{n}_2 s^2 + \underline{n}_1 s + \underline{n}_0 \right)$$

$$\Delta_{12} = \left(\underline{d}_7 s^8 + \overline{d}_6 s^7 + \overline{d}_5 s^6 + \underline{d}_4 s^5 + \underline{d}_3 s^4 + \overline{d}_2 s^3 + \overline{d}_1 s^2 + \underline{d}_0 s \right) + \left(k_d s^2 + k_p s + k_i \right)\left(\overline{n}_2 s^2 + \underline{n}_1 s + \underline{n}_0 \right)$$

$$\Delta_{13} = \left(\underline{d}_7 s^8 + \underline{d}_6 s^7 + \overline{d}_5 s^6 + \overline{d}_4 s^5 + \underline{d}_3 s^4 + \underline{d}_2 s^3 + \overline{d}_1 s^2 + \overline{d}_0 s \right) + \left(k_d s^2 + k_p s + k_i \right)\left(\underline{n}_2 s^2 + \overline{n}_1 s + \overline{n}_0 \right)$$

$$\Delta_{14} = \left(\overline{d}_7 s^8 + \overline{d}_6 s^7 + \underline{d}_5 s^6 + \underline{d}_4 s^5 + \overline{d}_3 s^4 + \overline{d}_2 s^3 + \underline{d}_1 s^2 + \underline{d}_0 s \right) + \left(k_d s^2 + k_p s + k_i \right)\left(\underline{n}_2 s^2 + \overline{n}_1 s + \overline{n}_0 \right)$$

$$\Delta_{15} = \left(\overline{d}_7 s^8 + \underline{d}_6 s^7 + \underline{d}_5 s^6 + \overline{d}_4 s^5 + \overline{d}_3 s^4 + \underline{d}_2 s^3 + \underline{d}_1 s^2 + \overline{d}_0 s \right) + \left(k_d s^2 + k_p s + k_i \right)\left(\underline{n}_2 s^2 + \overline{n}_1 s + \overline{n}_0 \right)$$

$$\Delta_{16} = \left(\underline{d}_7 s^8 + \overline{d}_6 s^7 + \overline{d}_5 s^6 + \underline{d}_4 s^5 + \underline{d}_3 s^4 + \overline{d}_2 s^3 + \overline{d}_1 s^2 + \underline{d}_0 s \right) + \left(k_d s^2 + k_p s + k_i \right)\left(\underline{n}_2 s^2 + \overline{n}_1 s + \overline{n}_0 \right)$$